Proceedings of the
Annual Stability Conference
Structural Stability Research Council
St. Louis, Missouri, April 16-20, 2013

Elastic Compressive Strength of Aluminum Open Circular-Arc Sections

C.M. Shepherd[1], R.D. Ziemian[2]

Abstract

Currently, the Specification for Aluminum Structures (Aluminum Association 2010) indicates thin-walled open circular-arc plate sections with radii greater than eight inches have a lower elastic compressive strength than a flat plate with the same width and thickness. This seems inconsistent with intuition, which would suggest any degree of plate folding should increase the elastic buckling strength. This paper will provide an overview of a study recently completed by the authors on a wide range of curvatures—from a nearly flat plate to semicircular. To quantify the curvature, a single non-dimensional parameter is used to represent all combinations of circumferential width, thickness, and radius. Employing the finite strip method (CU-FSM), elastic local buckling stresses are investigated. Based on the ratio of critical stress values of curved plates compared to flat plates of the same size, equivalent plate-buckling coefficients are computed. Using this data, nonlinear regression analyses are then performed to develop closed form capacity equations for five different edge support conditions. These expressions appear reasonable for calculating the elastic critical buckling stress for any open circular-arc section when the geometric properties (circumferential width, thickness, and radius) and the material properties (elastic modulus and Poisson's ratio) are known. Examples that show the applicability of these equations to circular-arc geometries other than those used as a basis for their development are also provided.

1. Introduction

1.1 Objective

Local buckling is an important failure mode to be considered particularly in the design of a structural compression member. Local buckling is identified by a portion of a structural shape (typically a web or flange) deflecting over a short region. The effects of local buckling are more severe with larger width-to-thickness ratios *b/t*.

Curved elements in extruded aluminum shapes are significantly more common than curved elements in steel due to the relative ease of fabrication. The current aluminum specification (Aluminum Association 2010) predicts that sections with radii greater than eight inches will have a lower strength capacity than an equivalent flat plate, which is inconsistent with intuition. In

[1] Graduate Student, Virginia Tech, <cmshep8@vt.edu>
[2] Professor, Bucknell University, <ziemian@bucknell.edu>

addition to investigating this inconsistency, this study serves to determine simple equations for computing the elastic critical buckling stress of an aluminum thin plate with a defined circumferential width, thickness, and radius when subject to uniform compression over a typical range of edge support conditions.

1.2 Scope

This study develops an expression for an equivalent plate buckling coefficient k_c^Z that can be used in the calculation of the elastic plate buckling stress σ_{cr}^Z for plates of open curved cross-section. This expression is a function of a non-dimensional variable Z that accounts for all pertinent geometric parameters of the plate, including circumferential width b, thickness t, and radius of curvature R (Fig. 1).

$$Z = \frac{b^2}{Rt} \tag{1}$$

Note that a flat plate can be represented by a curvature parameter Z equaling zero. Constants appearing in the derived k_c^Z expression are defined according to the five edge support conditions shown in Fig. 2.

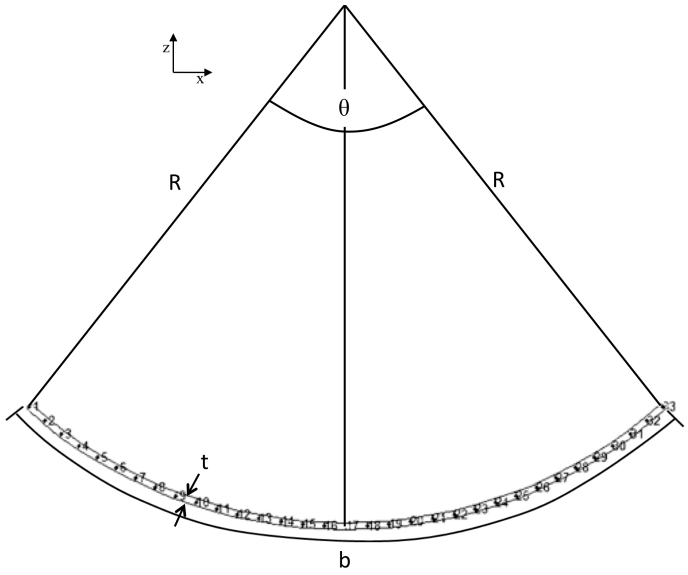

Figure 1: Geometric properties of curved plate sections used to calculate the curvature parameter *Z*.

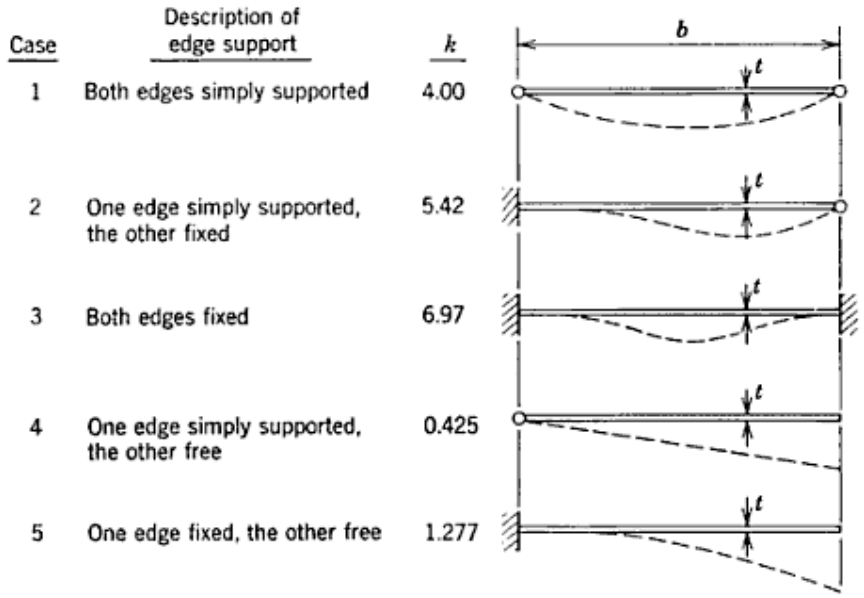

Figure 2: Edge support conditions considered in this study. Note that flat plate buckling coefficients $k = k_c^{plate}$ are also provided (Ziemian 2010).

2. Background

2.1 Theory

Local buckling can occur at stresses much lower than those at which member flexural and/or torsional buckling occurs. Due to the low moment of inertia and low initial resistance to out-of-plane deformations, thin-walled plate sections, like those often found in extruded aluminum shapes, are particularly susceptible to local buckling (White et al. 1974). Figure 3 shows examples of curved elements within popular aluminum structural shapes. Open sections, such as the one shown in the right of Fig. 3, are the primary focus of this paper.

Figure 3: Sample of aluminum curved shapes as they appear within structural shapes (Kissell 1995).

The elastic critical stress σ_{cr} of a transversely loaded flat plate is dependent on the width-to-thickness ratio *b/t* and longitudinal edge support conditions according to

$$\sigma_{cr} = k \frac{\pi^2 E}{12(1-\upsilon^2)\left(\frac{b}{t}\right)^2} \tag{2}$$

in which *k* is the plate buckling coefficient (Fig. 1), *E* is the elastic modulus of the material, and ν is Poisson's ratio (Ziemian 2010).

2.2 History

LeTran and Davaine (2011) investigated curved steel plates using extensive three-dimensional finite element studies based on shell elements. Their studies indicate that local buckling behavior depends on the radius of curvature, width-to-thickness ratio, and initial imperfections.

The four primary equations (Table 1) reviewed by LeTran and Davaine (2011) document the evolution of modeling curved plate behavior. These equations provide for calculating a buckling coefficient k_c^Z that includes curvature effects from which the elastic critical buckling stress σ_{cr}^Z can then be computed from

$$\sigma_{cr}^Z = k_c^Z \sigma_E \tag{3}$$

where σ_E is the elastic critical stress as defined in Eq. 2 with k = 1. LeTran and Davaine investigated buckling coefficients for the simply-supported edge-condition as proposed by Redshaw, Timoshenko, Stowell, and Domb and Leigh. The authors note (1) Redshaw and Stowell use similar forms to their equations, whereas Timoshenko makes an assumption on the form of the displacements, (2) Domb & Leigh's equation is calibrated using a curve fitting method, and (3) Stowell's is the only equation to account for different edge support conditions.

Table 1: Buckling coefficient formulas for curved panels (LeTran & Davaine 2011)

Author (Year)	Expression for buckling coefficient, k_c^Z
Redshaw (1933)	$2\left(1+\sqrt{1+\frac{12(1-\nu^2)}{\pi^4}Z^2}\right)$
Timoshenko (1961)	$\begin{cases} 4+\frac{3(1+\nu^2)}{\pi^4}Z^2 \; if \; Z \le \frac{2\pi^4}{\sqrt{3(1-\nu^2)}} \\ \frac{4\sqrt{3}}{\pi^2}Z^2 \; if \; Z \ge \frac{2\pi^4}{\sqrt{3(1-\nu^2)}} \end{cases}$
Stowell (1943)	$\frac{k_c^{plate}}{2}\left(1+\sqrt{1+\frac{48(1-\nu^2)}{\pi^4(k_c^{plate})^2}Z^2}\right)$
Domb and Leigh (2001)[1]	$\begin{cases} 10\sum_{i=0}^{3} c_i(\log Z_b)^i \; if \; 1 \le Z < 23.15 \\ c(Z)^d \; if \; 23.15 \le Z \le 200 \end{cases}$

[1]Where $Z_b=Z(1-\nu^2)$, c_0=0.6021, c_1=0.005377, c_2=0.192495, c_3=0.00267, c=0.4323, and d=0.9748

A recent literature survey found that little to no research into the behavior of aluminum open-curved plates could be located. In this regard, the *Specification for Aluminum Structures* (Aluminum Association 2010) has had to settle on employing the nominal capacity equations for closed circular and oval shapes when designing open curved shapes. Unfortunately, this results in the prediction that some open thin-walled circular-arc plate sections will have a lower elastic compressive strength than a flat plate of equivalent width and thickness. The study contained herein applies the knowledge from LeTran and Davaine's research on steel curved plate behavior with simple edge supports to an aluminum curved section with various combinations of edge support.

3. Discussion

3.1 Software

The elastic buckling behavior of thin-walled members can be modeled and analyzed through the use of CU-FSM (Schafer and Ádány 2006). This software employs the finite strip method—a specialized form of the finite element method—to find the buckling curve (buckling stress versus wave-length) of a particular cross section. Edge support conditions may be modeled by changing the restraint condition (fixed or free) at the nodal degrees of freedom. The minima of the buckling curves provide the half-wavelength and load factor for a given buckling mode. Because local buckling is the focus of this study, the buckling mode at the shortest half-wavelength is identified and used in subsequent analyses.

3.2 Inputs and Assumptions

To create the input geometries for CU-FSM, a constant width-to-thickness ratio *b/t* is maintained while the radius *R* is varied. In this study, the cross-section is comprised of 32 elements and subject to a uniform compressive stress of 1 ksi, thereby permitting the resulting buckling load ratio to be equivalent to the elastic critical buckling stress (ksi). In all analyses, initial imperfections are not considered. Input variables include the elastic modulus (E=10,100 ksi), Poisson's ratio (v=0.33), shear modulus (G=3,797 ksi), the coordinates and support conditions of each node, and the properties of the elements, including thickness and node connectivity

3.3 Methodology

In this research, CU-FSM is used to analyze open-curved plate sections for a series of twenty curvature Z values for each of five pairs of edge support conditions (pin-pin, fixed-free, fixed-fixed, pin-fixed and pin-free). To find the critical elastic buckling stress of interest, the entire buckling stress curve is reviewed in order to target the correct minimum, as more than one may exist (Fig. 4). The input wavelength range can be tailored to include the minimum of interest with a narrower range and smaller increment to obtain more precise results.

By combining the expression for the critical stress in a flat plate of arbitrary *b/t* and edge support condition (given by $\sigma_{cr}^{plate} = k_c^{plate}\sigma_E$) with Eq. 3, the equivalent curved plate buckling coefficient k_c^Z for the same *b/t* ratio and edge support condition may be defined in terms of the flat plate buckling coefficient k_c^{plate} and the critical stress ratio $\sigma_{cr}^Z/\sigma_{cr}^{plate}$ as follows

$$k_c^Z = k_c^{plate}\frac{\sigma_{cr}^Z}{\sigma_{cr}^{plate}} \tag{4}$$

By using CU-FSM to compute the elastic buckling stress σ_{cr}^Z over a wide range of curvature Z values, Eq. 4 may be used to plot the relationship between Z and the plate buckling coefficient k_c^Z for the edge support conditions being investigated.

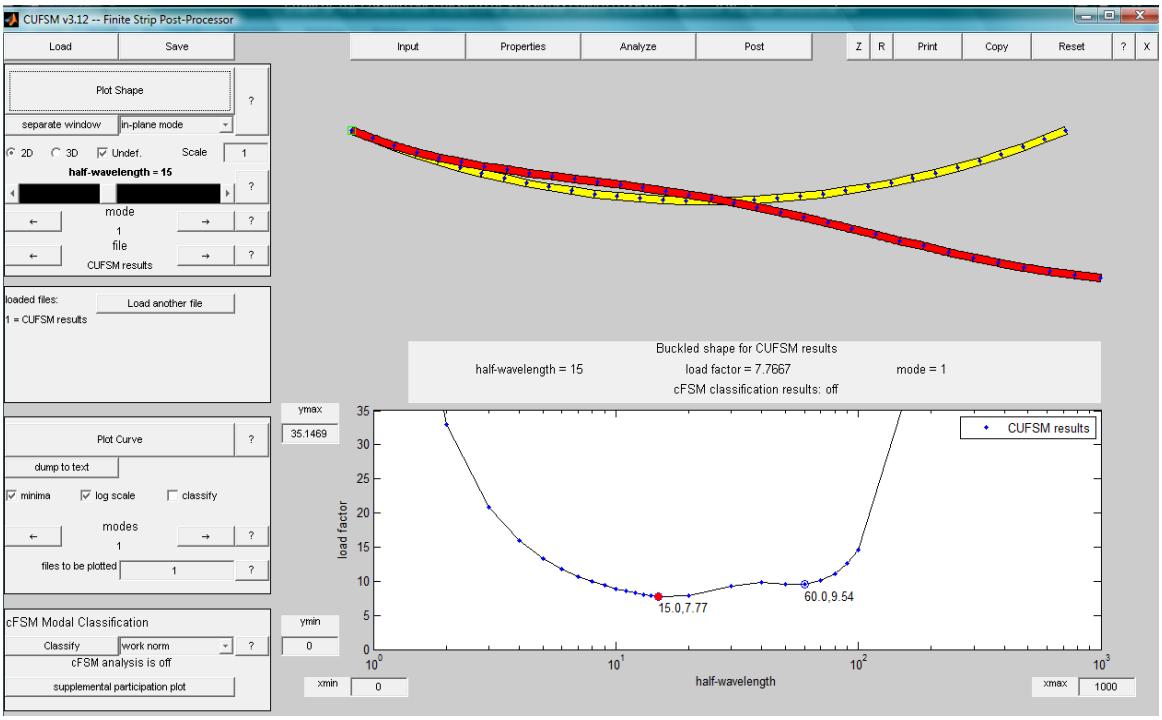

Figure 4: Screenshot of the CU-FSM results including buckled shape, half-wavelength and load factors

Before preparing plots of Eq. 4 for different edge support conditions, the fixed-free support condition was used to ensure the critical stress ratio $\sigma_{cr}^{Z}/\sigma_{cr}^{plate}$ is independent of *b*/*t*. Each of the *b/t* ratios provided in Table 2 were analyzed using CU-FSM over a wide range of curvature *Z* values and the resulting plots of Eq. 4 (Fig. 5) illustrate this invariance. With this in mind, only one *b/t* ratio and a wide range of radii need be analyzed for each of the edge support conditions.

Table 2: Geometries used to test different b/t ratios in CU-FSM

Width-to-thickness ratio, b/t	Width, b (inches)	Thickness, t (inches)
100	10	0.1
60	6	0.1
20	10	0.5

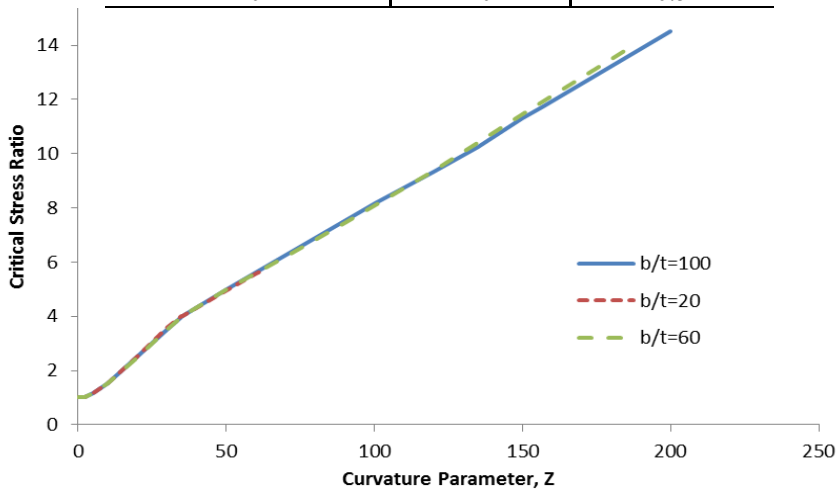

Figure 5: Critical stress ratios for fixed-free edge support condition analyzed with three b/t ratios

The range of curvature parameters investigated was from a nearly flat plate condition of Z=0.01 to a semi-circular section of Z=314 (Fig. 6).

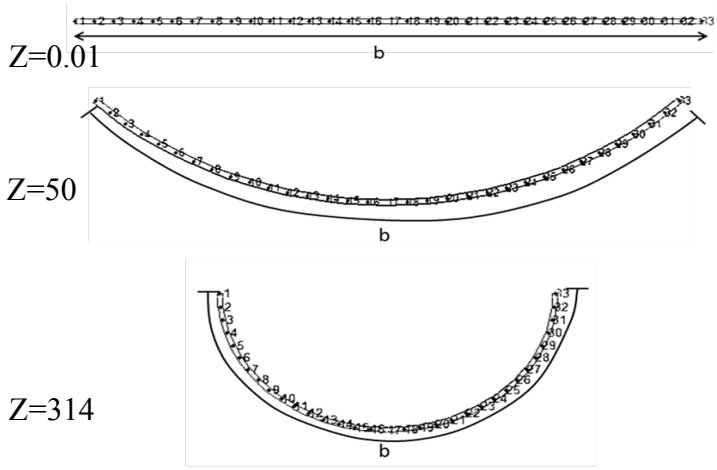

Figure 6: Range of curvature Z values investigated

3.4 Equation for Computing k_c^Z

CU-FSM data points for each edge support condition were plotted against the four equations listed in Table 1. The numerical results aligned best with Redshaw's equation for the buckling coefficient in the pin-pin edge support condition case (Fig. 7). Unfortunately, this equation does not account for other edge support conditions. As shown in Fig. 8 for the fixed-fixed edge support condition, the analysis results from CU-FSM align best with Stowell's curve for low Z-values, but trend towards Redshaw's curve at higher Z-values.

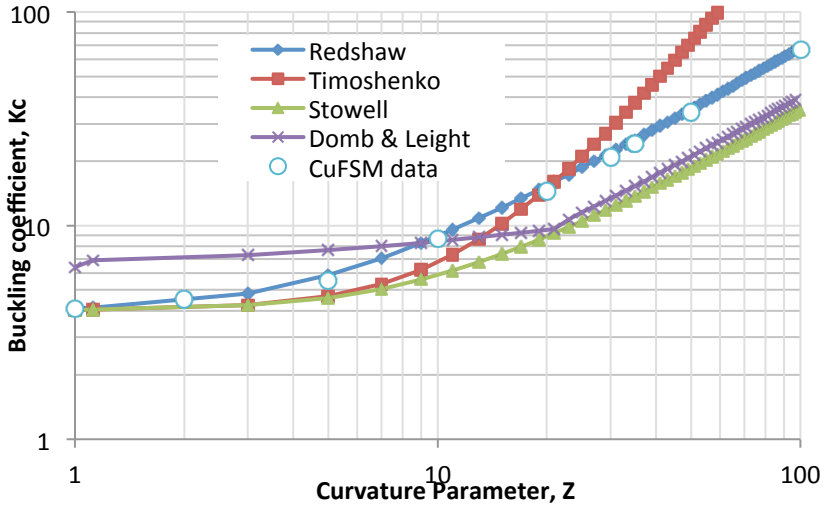

Figure 7: Previously considered equations (Table 1) for buckling coefficients verses CU-FSM results for the pin-pin edge support condition.

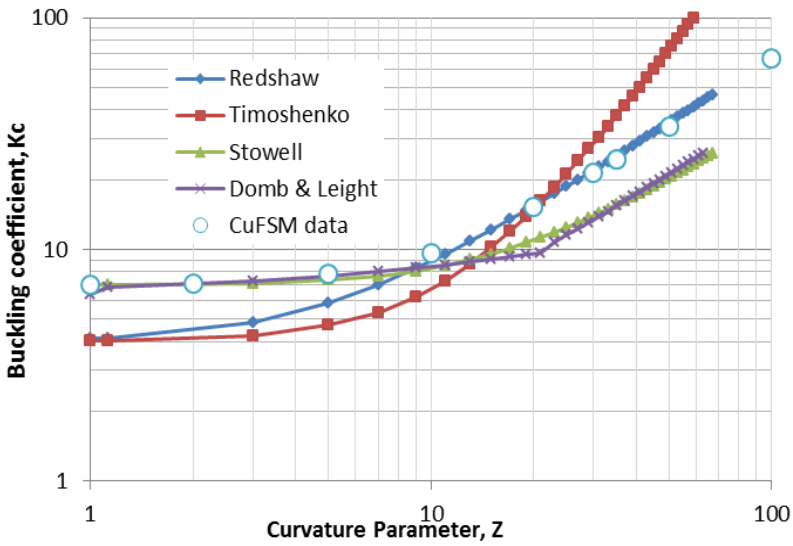

Figure 8: Previously considered equations (Table 1) for buckling coefficients verses CU-FSM results for the fixed-fixed edge support condition

Given that Redshaw's and Stowell's equations are of the same general form and the CU-FSM results agree with either depending on magnitude of Z, the basic form of Eq. 5 was selected for further study.

$$k_c^Z = A\left(1 + \sqrt{1 + BZ^2}\right) \tag{5}$$

Noting that at low curvature parameters (Z approximately equal to 0.0), flat plate behavior should be observed, the coefficient A was set equal to $0.5k_c^{plate}$, where k_c^{plate} is the flat plate buckling coefficient for the given edge support condition (Fig. 1). Using nonlinear regression analyses, the unknown B coefficients, which are function of the edge support condition, can then be obtained by fitting the numerical data to this equation.

To assess the regression analysis results, a coefficient of determination R^2 is calculated according to

$$R^2 = 1 - \frac{\Sigma(y_i - \bar{y})^2}{\Sigma(y_i - f_i)^2} = 1 - \frac{\Sigma(k_{c,i}^{Z,CU-FSM} - \bar{k}_c^{Z,CU-FSM})^2}{\Sigma(k_{c,i}^{Z,CU-FSM} - \bar{k}_c^{Z,Eq.\ 5})^2} \tag{6}$$

where y_i is the calculated k_c^Z from the CU-FSM data at a specific value of Z, $\bar{y}$ is the average of CU-FSM buckling coefficients for all Z-values, and f_i is the buckling coefficient as calculated from Eq. 5 for each of the corresponding Z-values.

4. Results

Detailed results for the five edge support conditions are provided in Appendix 1. In all cases, it can be observed that the critical buckling stress increases with increases in the curvature Z-parameter. That is, the critical buckling stress for a given b/t ratio will increase as the radius R of

the curved section decreases. Using the general form of Eq. 7, Table 2 provides values for obtained for B and their corresponding coefficients of determination R^2.

$$k_c^Z = \frac{k_c^{plate}}{2}\left(1 + \sqrt{1 + BZ^2}\right) \tag{7}$$

In all cases, R^2 values are very close to unity, thereby indicating good accuracy of Eq. 7 when combined with the B values obtained from the nonlinear regression analyses.

Table 2: Summary of results of nonlinear regression analysis

Edge support Condition	Plate Buckling Coefficient, k_c^{plate}	Calculated Parameter, B	Coefficient of Determination, R^2
Pin-Pin	4.0	0.1090	0.99983
Pin-Fixed	5.42	0.0587	0.99975
Fixed-Fixed	6.97	0.0349	0.99956
Fixed-Free	1.277	0.0201	0.99528
Pin-Free	0.425	0.1737	0.99118

As expected, the coefficient B = 0.1090 for the pin-pin edge support condition is nearly equal to the equivalent parameter contained within the Redshaw and Stowell equations (Table 1)

$$B_{Redshaw} = \frac{12(1-\nu^2)}{\pi^4} = 0.1098$$
$$B_{Stowell} = \frac{48(1-\nu^2)}{\pi^4\left(k_c^{plate}\right)^2} = 0.1097$$

The merit of this research, however, becomes more apparent when similar comparisons are made for other support conditions. For example, Table 2 provides a coefficient B = 0.0349 for the fixed-fixed case, whereas Redshaw and Stowell provide significantly different values of $B_{Redshaw}$ = 0.1098 and $B_{Stowell}$ = 0.00904. The largest difference is observed for the fixed-free case with B = 0.0201, and $B_{Redshaw}$ = 0.1098 and $B_{Stowell}$ = 0.2693. It is noted that in all cases, the Redshaw equation does not account for variation in edge support conditions.

Fig. 9 shows plots of the buckling coefficient curves obtained from regression analyses for all five edge support conditions over a wide range of Z-values. As expected, each curve intercepts the vertical axis at the flat plate-buckling coefficient k_c^{plate} associated with its edge support condition.

From Eq. 4, the critical buckling stress ratio $\sigma_{cr}^Z/\sigma_{cr}^{plate}$ may be defined as the ratio of the plate buckling coefficients

$$\frac{\sigma_{cr}^Z}{\sigma_{cr}^{plate}} = \frac{k_{cr}^Z}{k_{cr}^{plate}} \tag{8}$$

With this in mind, normalizing each of the curves shown in Fig. 9 by the corresponding flat plate-buckling coefficient k_c^{plate} results in the critical buckling stress ratio $\sigma_{cr}^Z/\sigma_{cr}^{plate}$ curves provided Fig. 10. Two important factors may be observed, including (1) any amount of

curvature in the plate results in an increase plate buckling resistance, and (2) for a given Z value, the largest increase in capacity resulting from moving from a flat plate to a curved plate of the same cross-sectional area will occur for the pin-free edge combination, the smallest increase will be for the fixed-free case, and with increases for the remaining edge support conditions shown in the figure.

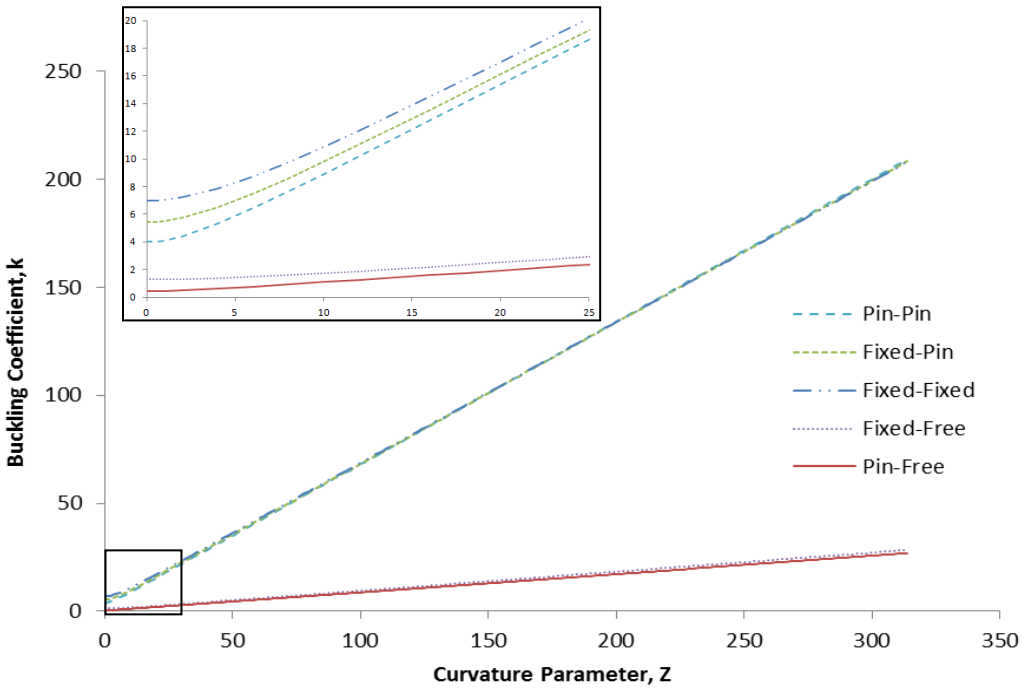

Figure 9: Buckling coefficients from nonlinear regression analysis versus curvature parameter, Z for each edge support condition considered in this study

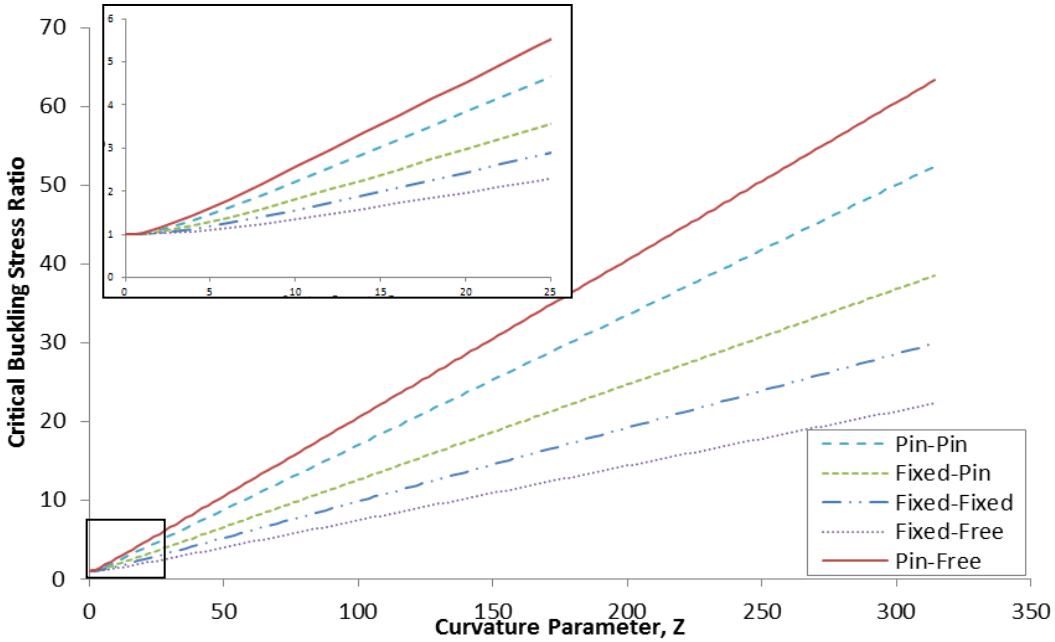

Figure 10: Critical buckling stress ratios versus curvature parameter for all five edge support conditions

5. Examples

Two examples are presented to illustrate the use and show the accuracy of Eqs. 3 and 5. For the geometry shown in Fig. 11, Eqs. 1 and 2 (with $k = 1$) result in a $Z = 15$ and $\sigma_E = 10.36$ksi. With these values, curved plate buckling coefficients and stresses computed using Eqs. 3 and 5, respectively, are provided in Table 3 for typical edge support conditions. Using the same approach to assess the geometry shown in Fig. 12 and with $Z = 750$ and $\sigma_E = 0.1036$ksi, the results provided in Table 4 are obtained. In both tables, comparisons with the theoretical exact solutions obtained by CU-FSM are also provided and indicate that accurate results are obtained by Eq. 4.

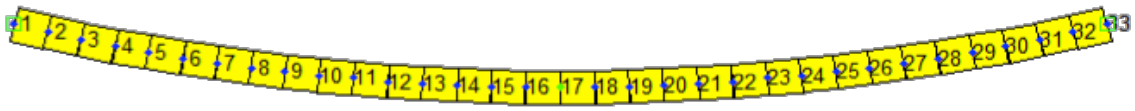

Figure 11: Aluminum circular curved section with $t = 0.1$ in., $b = 12$ in., $R = 24$ in., $E = 10{,}100$ksi, and $v = 0.33$.

Table 3: Results obtained for the geometry shown in Fig. 13.

Edge Support Condition	k_c^{plate}	B	k_c^Z	σ_c^Z (ksi)	$\sigma_c^{Z,\ CUFSM}$ (ksi)	% Error
Pin-Pin	4	0.109	41.669	26.975	26.1839	3.021
Pin-Fixed	5.42	0.0587	42.198	27.318	26.2247	4.167
Fixed-Fixed	6.97	0.0349	42.703	27.645	26.2723	5.224
Fixed-Free	1.277	0.0201	6.107	3.954	4.519	12.510
Pin-Free	0.425	0.1737	5.531	3.580	4.1639	14.015

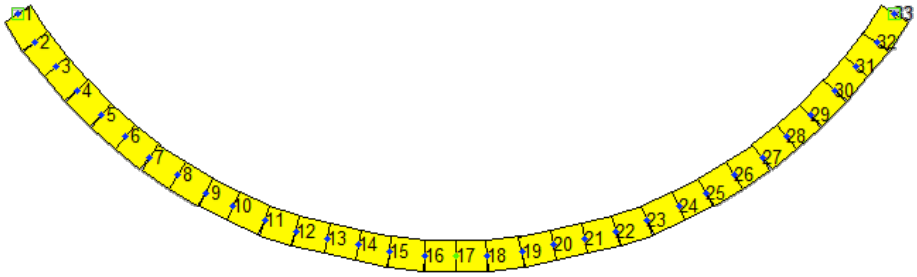

Figure 12: Aluminum circular curved section with $t = 0.1$ in., $b = 30$ in., $R = 12$ in., $E = 10{,}100$ksi, and $v = 0.33$.

Table 4: Results obtained for the geometry shown in Fig. 13.

Edge Support Condition	k_c^{plate}	B	k_c^Z	σ_c^Z (ksi)	$\sigma_c^{Z,\ CUFSM}$ (ksi)	% Error
Pin-Pin	4	0.109	497.231	51.503	53.4402	3.626
Pin-Fixed	5.42	0.0587	495.153	51.287	53.4414	4.031
Fixed-Fixed	6.97	0.0349	491.786	50.939	53.4426	4.685
Fixed-Free	1.277	0.0201	68.534	7.099	6.3591	11.630
Pin-Free	0.425	0.1737	66.636	6.902	6.2962	9.623

6. Summary

By performing more than one hundred CU-FSM finite strip analyses, the theoretical elastic critical buckling stresses of curved aluminum plates over a variety of curvatures and edge support conditions are provided. Employing concepts presented by LeTran and Davaine (2011), who investigated steel curved plates with pin-pin edge supports, nonlinear regression analyses are used to develop accurate closed-form expressions for curved plate buckling coefficients k_c^Z and elastic critical buckling stresses σ_{cr}^Z. These relatively simple equations are based on a geometrical parameter Z, which is a function of the plate's curvature R, width b, and thickness t.

This study only investigated the perfect edge support conditions shown in Fig. 1. In many cases, such as the open section shown in Fig. 3, the degree of edge support restraint is somewhere between ideal conditions. Until such research is completed, Fig. 10 may be used to define the upper and lower bounds of the elastic critical buckling stress and approximations may be made via an interpolation based on an estimate of the degree of rotational restraint provided at the edges.

It is also important to note that this study did not consider the effects of initial imperfections, which have been shown to impact the local buckling capacity of closed circular and oval shapes (Ziemian 2010). Of course, there may also exist the possibility of some increase in capacity resulting from post-buckling strength, especially for plates with small amounts of curvature (nearly flat). With this in mind, the next step in this research will be to assess the impact of such effects on the strength of open curved sections. Unfortunately, this will require moving away from the relatively easy to employ CU-FSM software (due to the corresponding limitations in the finite strip method) and into the use of more complex three-dimensional finite element analyses that most likely employ shell elements.

Acknowledgements
The authors would like to thank the Aluminum Association for sponsoring this research and especially, J. Randolph Kissell of The TGB Partnership for his invaluable assistance. The views expressed in this paper are solely those of the authors and may not represent the positions of the aforementioned organization or individual.

References

Aluminum Association (2010). *Specification for Aluminum Structures*, Arlington, VA.

Kissell, J., and Ferry, R. (1995). *Aluminum Structures: A guide to their specifications and design.* John Wiley & Sons, Inc., NY.

Le Tran, K., and Davaine, L. (2012). "Stability of Curved Panels under Uniform Axial Compression." *Journal of Constructional Steel Research*. 69(1), 30–38.

Schafer, B., and Ádány, S. (2006). "Buckling analysis of cold-formed steel members using CUFSM: conventional and constrained finite strip methods." *Eighteenth International Specialty Conference on Cold-Formed Steel Structures*, Orlando, FL.

White, R., Gergely, P., and Sexsmith, R. (1974). *Structural Engineering, Vol. 3, Behavior of Members and Systems*. John Wiley & Sons, Inc., NY.

Ziemian, R. Ed. (2010). *Guide to Stability Design Criteria for Metal Structures*. 6th ed. John Wiley & Sons, Hoboken, NJ

Appendix

The following sections contain the numerical data obtained for the various edge support conditions investigated.

A.1 Pin-Pin

$$k_{c,pin-pin}^{Z} = \frac{4}{2}\left(1 + \sqrt{0.109Z^2}\right)$$

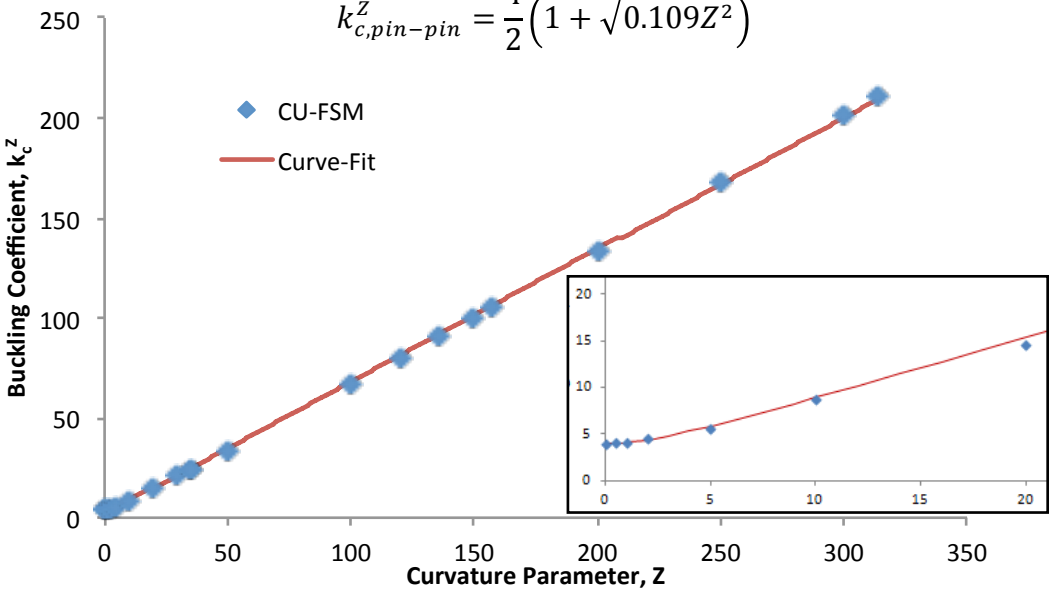

Figure A1: Plot of CU-FSM data and the nonlinear regression curve for the pin-pin edge support condition.

Table A1: CU-FSM results with output from the nonlinear regression for the pin-pin edge support condition.

	$B_{pin\text{-}pin}$= 0.1090		R^2= 0.9998	
Curvature Parameter, Z	Critical Buckling Stress (ksi), $\sigma_{cr,\ CU\text{-}FSM}$	Half Wavelength (in)	Buckling Coefficient from CU-FSM, $k_{c,CU-FSM}^{Z}$	Buckling Coefficient from Eq. 7, k_c^Z
0.01	3.7288	10	4.000	4.000
0.5	3.8106	9.8	4.088	4.027
1	3.7927	9.9	4.069	4.106
2	4.2167	8.9	4.523	4.397
5	5.1463	7.6	5.521	5.860
10	8.0892	5.5	8.677	8.899
20	13.562	4.1	14.55	15.36
30	19.473	3.3	20.89	21.91
35	22.5	3.1	24.14	25.20
50	31.5973	2.6	33.90	35.08
100	62.215	1.8	66.74	68.06
120	74.9218	1.6	80.37	81.26
135	83.9449	1.5	90.05	91.16
150	93.2204	1.5	100.0	101.1
157	97.6299	1.4	104.7	105.7
200	124.7926	1.3	133.9	134.1
250	156.3662	1.1	167.7	167.1
300	188.0642	1	201.7	200.1
314	196.4419	1	210.2	209.3

A.2 Pin-Fixed

$$k_{c,pin-fixed}^{Z} = \frac{5.42}{2}\left(1+\sqrt{0.0587Z^2}\right)$$

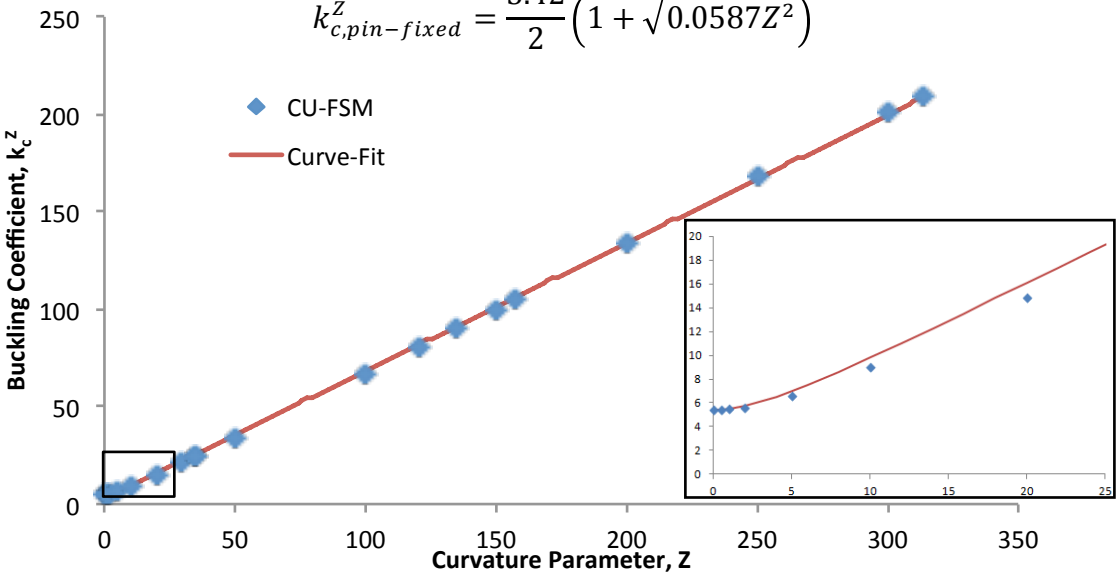

Figure A2: Plot of CU-FSM data and the nonlinear regression curve for the pin-fixed edge support condition.

Table A2: CU-FSM results with output from the nonlinear regression for the pin-fixed edge support condition.

	$B_{pin\text{-}fixed}$= 0.0587		R^2= 0.9997	
Curvature Parameter, Z	Critical Buckling Stress (ksi), $\sigma_{cr,\ CU\text{-}FSM}$	Half Wavelength (in)	Buckling Coefficient from CU-FSM, $k_{c,CU-FSM}^{Z}$	Buckling Coefficient from Eq. 7, k_c^Z
0.01	5.0432	8	5.410	5.420
0.5	5.0727	7.9	5.442	5.440
1	5.11	7.9	5.482	5.498
2	5.2406	7.7	5.622	5.721
5	6.1209	6.9	6.566	6.967
10	8.3569	5.9	8.965	9.813
20	13.8694	4.1	14.878	16.118
30	19.5937	3.4	21.019	22.593
35	22.6863	3.1	24.336	25.850
50	31.6976	2.6	33.952	35.651
100	62.3161	1.8	66.848	68.424
120	74.7024	1.6	80.135	81.546
135	84.4738	1.5	90.617	91.390
150	93.2204	1.5	99.972	101.234
157	97.7094	1.4	104.815	105.829
200	124.6699	1.3	133.736	134.054
250	156.2851	1.1	167.650	166.878
300	187.2006	1.3	200.814	199.703
314	196.4421	1	209.197	208.894

A.3 Fixed-Fixed

$$k_{c,fixed-fixed}^{Z} = \frac{6.97}{2}\left(1+\sqrt{0.0349Z^2}\right)$$

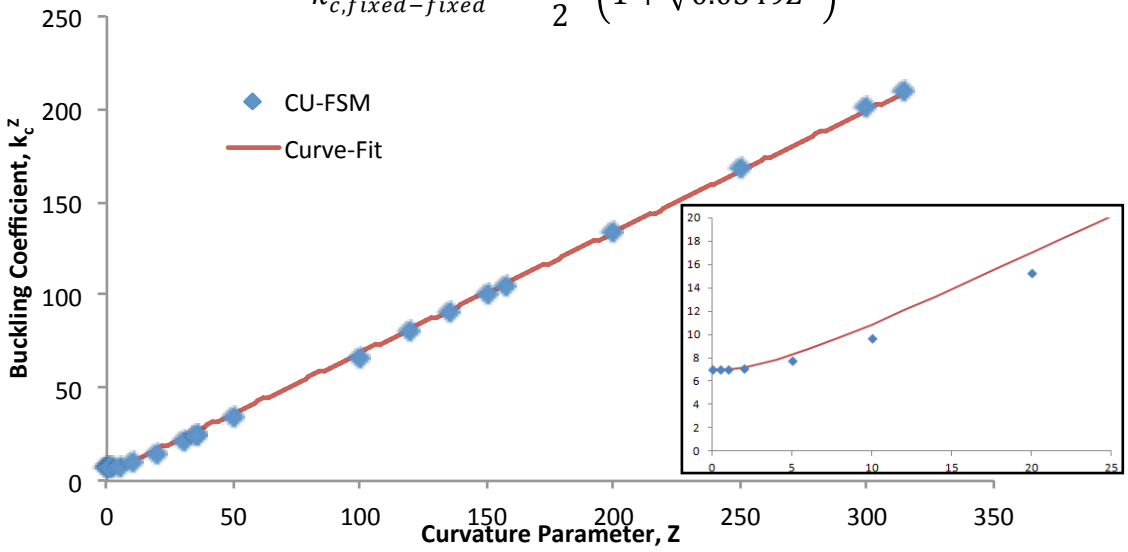

Figure A3: Plot of CU-FSM data and the nonlinear regression curve for the fixed-fixed edge support condition.

Table A3: CU-FSM results with output from the nonlinear regression for the fixed-fixed edge support condition.

	$B_{fixed\text{-}fixed}$= 0.0349		R^2= 0.9995	
Curvature Parameter, Z	Critical Buckling Stress (ksi), $\sigma_{cr,\ CU\text{-}FSM}$	Half Wavelength (in)	Buckling Coefficient from CU-FSM, $k_{c,CU-FSM}^{Z}$	Buckling Coefficient from Eq. 7, k_c^Z
0.01	6.4984	6.6	6.970	6.970
0.5	6.5256	6.6	6.999	6.985
1	6.5445	6.6	7.019	7.030
2	6.6192	6.5	7.100	7.205
5	7.2624	6.1	7.789	8.254
10	9.0214	5.3	9.676	10.870
20	14.2523	4.1	15.287	16.964
30	19.8264	3.4	21.265	23.325
35	22.883	3.1	24.544	26.537
50	31.8309	2.6	34.040	36.224
100	62.3228	1.8	66.846	68.683
120	74.7301	1.6	80.153	81.689
135	84.512	1.5	90.645	91.446
150	93.2205	1.5	99.963	101.205
157	97.7152	1.4	104.807	105.760
200	124.6852	1.3	133.734	133.742
250	156.3013	1.1	167.644	166.285
300	187.2535	1.3	200.843	198.832
314	196.4423	1	209.198	207.945

A.4 Fixed-Free

$$k_{c,fixed-free}^{Z} = \frac{1.277}{2}\left(1+\sqrt{0.0201Z^2}\right)$$

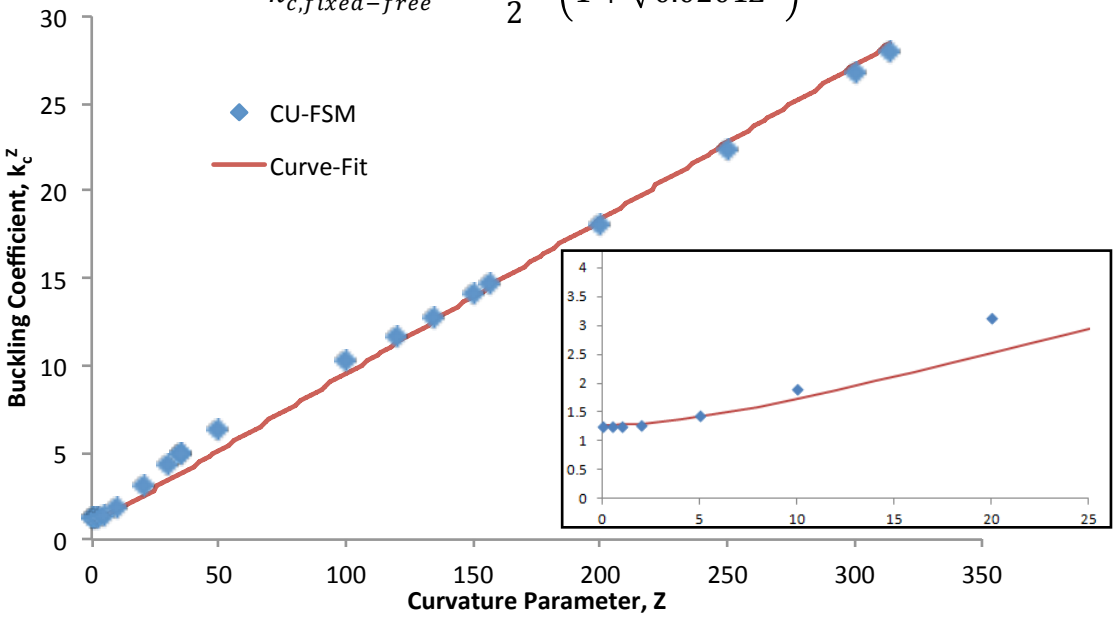

Figure A4: Plot of CU-FSM data and the nonlinear regression curve for the fixed-free edge support condition.

Table A4: CU-FSM results with output from the nonlinear regression for the fixed-free edge support condition.

	$B_{fixed\text{-}free}$= 0.0201		R^2= 0.9952	
Curvature Parameter, Z	Critical Buckling Stress (ksi), $\sigma_{cr,\ CU\text{-}FSM}$	Half Wavelength (in)	Buckling Coefficient from CU-FSM, $k_{c,CU-FSM}^{Z}$	Buckling Coefficient from Eq. 7, k_c^Z
0.01	1.165	16.4	1.277	1.277
0.5	1.1688	16.4	1.281	1.279
1	1.1738	16.5	1.287	1.283
2	1.1901	16.6	1.305	1.302
5	1.337	17.6	1.466	1.421
10	1.7616	20.7	1.931	1.746
20	2.9144	28.7	3.195	2.558
30	4.0771	35.1	4.469	3.428
35	4.6601	14	5.108	3.871
50	5.8174	14.8	6.361	5.209
100	9.5329	18.9	10.449	9.713
120	10.8655	20	11.910	11.520
135	11.9208	21	13.067	12.876
150	13.1899	22.2	14.458	14.232
157	13.6911	22.6	15.007	14.865
200	16.8934	25.1	18.517	18.754
250	20.8061	27.5	22.806	23.278
300	24.9831	30.1	27.385	27.803
314	26.2607	30.8	28.785	29.070

A.5 Pin-Free

$$k_{c,pin-free}^{Z} = \frac{0.425}{2}\left(1+\sqrt{0.1737Z^2}\right)$$

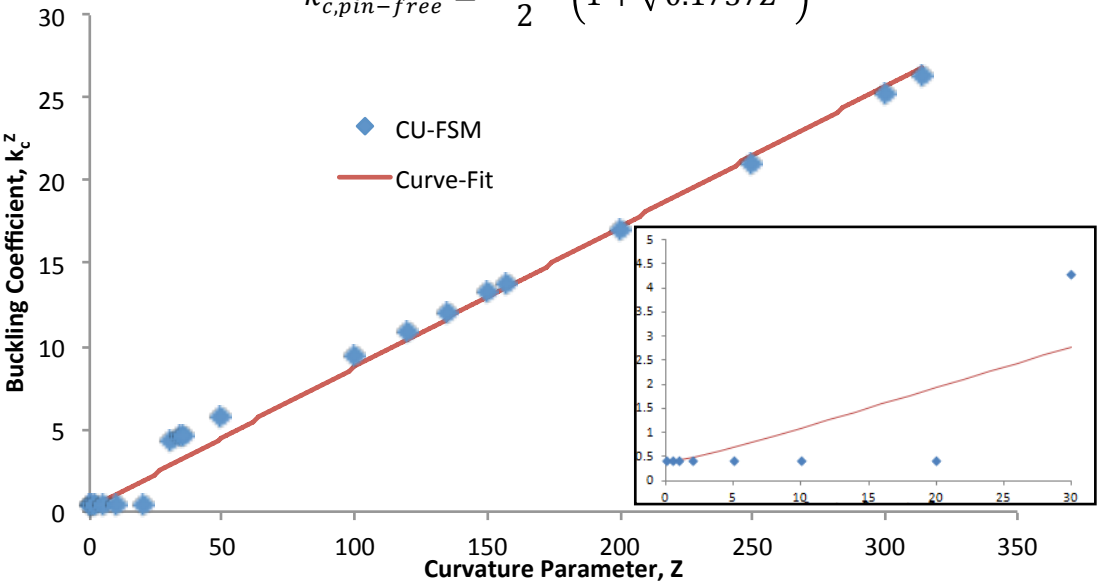

Figure A5: Plot of CU-FSM data and the nonlinear regression curve for the pin-free edge support condition.

Table A5: CU-FSM results with output from the nonlinear regression for the pin-free edge support condition.

	$B_{pin\text{-}free}$= 0.1737		R^2= 0.9911	
Curvature Parameter, Z	Critical Buckling Stress (ksi), $\sigma_{cr,\ CU\text{-}FSM}$	Half Wavelength (in)	Buckling Coefficient from CU-FSM, $k_{c,CU-FSM}^{Z}$	Buckling Coefficient from Eq. 7, k_c^Z
0.01	0.38045	345	0.425	0.425
0.5	0.38001	535	0.425	0.430
1	0.37986	731	0.424	0.443
2	0.37989	690	0.424	0.489
5	0.3798	834	0.424	0.704
10	0.38076	1097	0.425	1.123
20	0.38234	1295	0.427	1.996
30	3.9918	15.2	4.459	2.878
35	4.2933	15.2	4.796	3.320
50	5.3421	16.9	5.946	4.646
100	8.8551	22.5	9.892	9.071
120	10.1664	24.2	11.357	10.842
135	11.1874	25.5	12.497	12.171
150	12.3737	27.1	13.823	13.499
157	12.8493	27.6	14.354	14.119
200	15.9141	31	17.778	17.927
250	19.6685	34.8	21.972	22.355
300	23.5619	38.6	26.321	26.783
314	24.7396	39.6	27.444	28.023